Quaternary International 598 (2021) 24–37

Contents lists available at ScienceDirect

Quaternary International

journal homepage: www.elsevier.com/locate/quaint

Biochronostratigraphy of the western equatorial Atlantic for the last 1.93 Ma

Fabricio Ferreira [a,b,*], Cleverson G. Silva [b], Allan S. Oliveira [b], Cristiano M. Chiessi [c], Andrea K. Kern [d], Paul A. Baker [e], Gary Dwyer [e], Catherine A. Rigsby [f], Enqing Huang [g], Jun Tian [g]

[a] Postgraduate Program in Ocean and Earth Dynamics, Institute of Geosciences, Universidade Federal Fluminense, Av. Gal. Milton Tavares de Souza s/n, CEP: 24210-346, Niterói, RJ, Brazil
[b] Marine Geology Laboratory (LAGEMAR), Institute of Geosciences, Universidade Federal Fluminense, Av. Gal. Milton Tavares de Souza s/n, CEP: 24210-346, Niterói, RJ, Brazil
[c] School of Arts, Sciences and Humanities, University of São Paulo, Av. ArlindoBettio 1000, CEP: 03828-000, São Paulo, SP, Brazil
[d] Department of Sedimentary and Environmental Geology, Institute of Geosciences, University of São Paulo, Rua do Lago 562, CEP: 05508-080, São Paulo, SP, Brazil
[e] Division of Earth and Ocean Sciences, Duke University, NC 27708, Durham, USA
[f] Department of Geological Sciences, East Carolina University, NC 27858-4353, Greenville, USA
[g] State Key Laboratory of Marine Geology, Tongji University, 1239 Siping Road, 200092, Shanghai, China

ARTICLE INFO

Keywords:
Planktonic foraminifera
Biostratigraphy
Equatorial western Atlantic
Brazilian equatorial margin
Pará-Maranhão Basin

ABSTRACT

Planktonic foraminifera are an important biochronostratigraphic tool and one of the main proxies used in paleoceanographic studies. Here we present the integration of quantitative analyses of planktonic foraminifera biostratigraphy, planktonic and benthic foraminifera oxygen isotopic data, and planktonic foraminifera radiocarbon ages in a biochronostratigraphic framework for the last 1.93 Ma of the western equatorial Atlantic. The ages of the biostratigraphic events derived from our records are consistent with previous works except for the highest occurrences of *Globigerinoidesella fistulosa* (~1.82 Ma; MIS 66), *Globigerinoides obliquus* (~1.48 Ma; MIS 49), *Globorotalia tosaensis* (~1.05 Ma; MIS 31), and *G. viola* (~0.34 Ma; MIS 10). The largest difference in age (~1.13 Ma) was found for the highest occurrence of *G. viola*. In addition, we describe for the first time in the equatorial and western South Atlantic the oldest Pleistocene *Globorotalia menardii* disappearance (D) and reappearance (R) events D5 (~1.79 Ma; MIS 64), R5 (~1.68 Ma; MIS 60), D4 (~1.05 Ma; MIS 30) and R4 (~0.96 Ma; MIS 26). Our records present a consistent difference in the ages of *G. menardii* D and R events compared to the North and South Atlantic. While the onset of D events occurs initially at high latitudes and later in the equatorial region, the timing of R events exhibit the opposite trend. The oscillations in abundance of the complexes *Pulleniatina* and *Globorotalia crassaformis* together with the species *Globorotalia truncatulinoides* and *Globoconella inflata* allowed the subdivision of the last 1.93 Ma into 20 subzones, substantially improving the biochronostratigraphic resolution for the western equatorial Atlantic.

1. Introduction

Robust stratigraphic correlations within and between different oceanic basins are essential to deciphering the evolution of various components of the Earth system (Wade et al., 2011). Due to their high sensitivity to environmental conditions, high morphological diversity, global distributions, rapid evolution throughout the Mesozoic and Cenozoic, and high preservation potential, planktonic foraminifera are ideal biostratigraphic index fossils (Wade et al., 2011). Throughout the Cenozoic, planktonic foraminifera are an abundant and diverse microfossil group in the tropics and subtropics, and the evolutionary events of this group are used to set biozone boundaries, allowing the construction of detailed zonal schemes for the last 65 Ma (Blow, 1969; Bolli and Premoli Silva, 1973; Kennett and Srinivasan, 1983; Bolli and Saunders, 1985; Wade et al., 2011).

In addition to first and last occurrences of planktonic foraminifera

* Corresponding author. Postgraduate Program in Ocean and Earth Dynamics, Institute of Geosciences, Universidade Federal Fluminense, Av. Gal. Milton Tavares de Souza s/n, CEP: 24210-346, Niterói, RJ, Brazil.
E-mail address: ferreira_paleo@hotmail.com (F. Ferreira).

https://doi.org/10.1016/j.quaint.2021.04.042
Received 4 November 2020; Received in revised form 25 April 2021; Accepted 29 April 2021
Available online 6 May 2021

species (ten new appearances and seven disappearances of taxons; Wade et al., 2011) described for the Quaternary (last 2.58 Ma, Gibbard et al., 2010), glacial/interglacial climatic oscillations caused significant expansions and contractions in the geographic distribution of certain assemblages and/or species due to migration events with non-evolutionary characteristics (Kennett and Huddlestun, 1972; Bé et al., 1976; Thunnel, 1984; Caley et al., 2012). These changes in the relative abundance of assemblages and/or species of planktonic foraminifera themselves can provide an increased resolution of stratigraphic zoning during the Quaternary (Ericson and Wollin, 1968; Kennett and Huddlestun, 1972; Martin et al., 1993; Kohl et al., 2004; Ferreira et al., 2012; Toledo et al., 2016).

Yet, Quaternary biochronostratigraphical studies are scarce in the western equatorial Atlantic (e.g., Chaisson and Pearson, 1997), despite the great relevance of the region as an archive of climate variability of tropical South America (Arz et al., 1998; Nace et al., 2014; Zhang et al., 2017; Crivellari et al., 2018). Here, we present the integration of quantitative analyses of planktonic foraminifera biostratigraphy, calibrated with planktonic and benthic foraminifera oxygen isotopic records and radiocarbon ages for the last 1.93 Ma in a core with an average accumaltion rate around 3.35 cm/ka.

2. Study area

The modern surface ocean circulation in the western equatorial Atlantic is dominated by the North Brazil Current (NBC) and the North Equatorial Countercurrent. The NBC results from the bifurcation of the South Equatorial Current at 10–15°S. The NBC flows northwestwards along the continental margin of northeastern Brazil (Fig. 1; Peterson and Stramma, 1991; Schott et al., 1995; Stramma et al., 1995). The southward flowing Brazil Current also originates at the bifurcation and subsequently moves southward along the continental margin of eastern Brazil. With its large anticyclonic rings, the NBC is the main pathway for the cross-equatorial transport of warm and salty surface waters that balances the southward export of North Atlantic Deep Water (Johns et al., 1998; Goni and Johns, 2001; Haarsma et al., 2011). The NBC extends from the surface to intermediate water depths (approximately 800 m water depth) where it merges with northward advected Antarctic Intermediate Water (Talley et al., 2011). In the region of core CDH-79, long-term annual mean sea surface temperature is 27.5 °C (between 27.3 °C and 28.2 °C) (Locarnini et al., 2018), while sea surface salinity is 35.7 (varying widely between 28.2 and 36.2) (Zweng et al., 2018).

The NBC transport is highly variable, with maximum and minimum measured transport of approximately 36 Sv during the austral winter and 13 Sv during the austral fall (Johns et al., 1998). This variability in NBC transport is associated with the north-south migration of the Intertropical Convergence Zone and with changes in wind stress curl (Richardson et al., 1994; Talley et al., 2011). Between July and February, the NBC detaches from the continental margin at approximately 8°N feeding the North Equatorial Countercurrent in a process known as the NBC retroflection (Fonseca et al., 2004). Between March and June, the NBC flow continues farther northwestward along the continental slope of South America, entering the Caribbean Sea and eventually feeding the Gulf Stream (Johns et al., 1998; Lux et al., 2001).

The NBC transport variability is also observed on different timescales and correlates positively with the strength of Atlantic meridional overturning circulation (AMOC) on decadal timescale (Zhang et al., 2011). On millennial timescales, decreases in NBC strength coincided with northern Hemisphere cold events like the Heinrich stadials and the Younger Dryas (Arz et al., 1999; Wilson et al., 2011; Nace et al., 2014; Zhang et al., 2015).

3. Material and methods

We investigated core CDH-79 (00° 39.6853′ N, 44° 20.7723′ W; 32.12 m core length; 2345 m water depth; Fig. 1), retrieved during RV Knorr cruise KNR 197–4 in February 2010. The coring site is located on the top of a seamount in the western equatorial Atlantic (Pará-Maranhão Basin), 320 km from the modern coastline of northeastern Brazil. Core CDH-79 was shipped to Woods Hole Oceanographic Institution for storage at 4 °C. The working halves of the split cores were visually described and sampled (10 cm^3) every 10 cm for a total of 322 samples.

3.1. Preparation of planktonic foraminifera

The unlithified sediment samples were washed through a sieve of 62

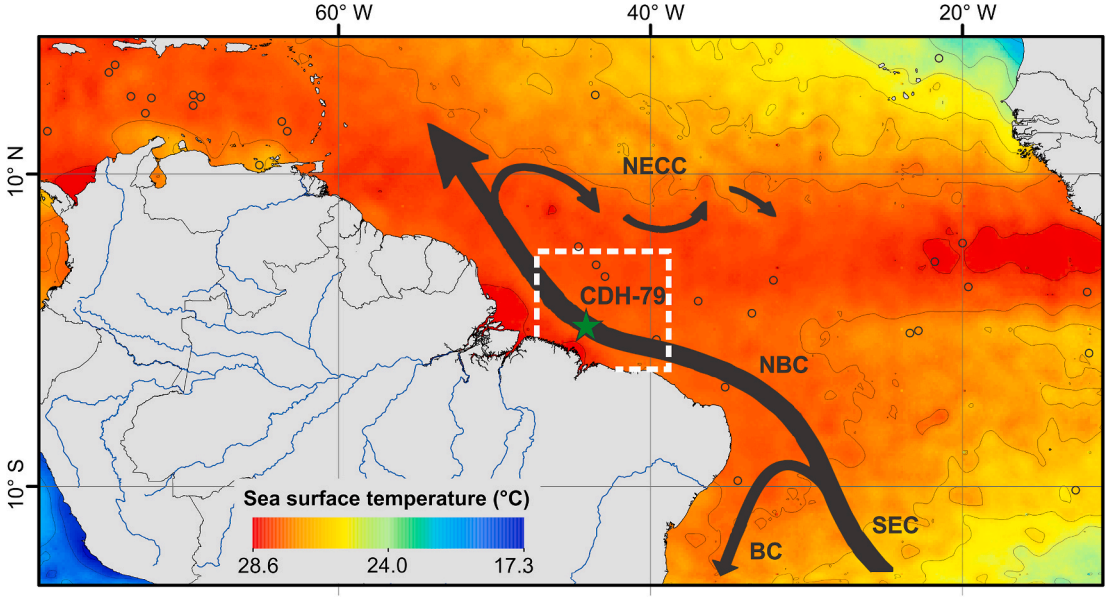

Fig. 1. Location of marine sediment core CDH-79 (green star) with long-term mean annual sea surface temperature (color scale) (Locarnini et al., 2018) and surface ocean currents of interest for this study (black arrows). The white dashed rectangle indicates the area used to estimate the long term mean sea surface temperature for the study area. The white circles represent sites discussed in the text (see Table S1 and Fig. S1 for details). BC - Brazil Current; NBC - North Brazil Current; NECC - North Equatorial Countercurrent; SEC - South Equatorial Current (Peterson and Stramma, 1991). (For interpretation of the references to color in this figure legend, the reader is referred to the Web version of this article.)

μm mesh size (retaining the coarse fraction) and dried at 50 °C (Leipnitz et al., 2005). Dry residues were weighed and stored in glass vials. Planktonic foraminifera were dry picked from the >150 μm fraction in subsample splits (if necessary) containing 300–600 specimens. This results in a 95% level of confidence for species with at least 1% of abundance (Patterson and Fishbein, 1989). The subsamples were stored in micropaleontological slides and all specimens were identified and counted. The specimen preservation was qualitatively estimated and the Le and Shackleton (1992) fragmentation index (FRAG) was calculated for each sample. The taxonomic concepts for Neogene taxa were adopted from Stainforth et al. (1975), Kennett and Srinivasan (1983), Bolli and Saunders (1985) and revised based on Hayward et al. (2019). The taxonomic terms that were utilized are available in Table S2.

3.2. Planktonic foraminifera biostratigraphy

Only species significant for Quaternary biostratigraphy were considered for the construction of the biostratigraphic framework (e.g., Ericson and Wollin, 1968; Berggren et al., 1985a, 1995a; 1995b; Wade et al., 2011; Toledo et al., 2016). The biostratigraphic zonal scheme for the Neogene followed Blow (1969), modified by Kennett and Srinivasan (1983). The Quaternary biostratigraphic zonal scheme followed Bolli and Premili Silva (1973), with the modifications from Bolli and Saunders (1985), Berggren et al. (1995a, 1995b) and the revision of the Cenozoic tropical biostratigraphy presented by Wade et al. (2011). The nomenclature adopted for evolutionary events, new appearance and disappearance of the taxon follow Wade et al. (2011), where lowest occurrence (LO) is used with the same meaning as first appearance datum and/or first occurrence. Similarly, the highest occurrence (HO) is used with the same meaning as the last appearance datum and/or the last occurrence. Following Wade et al. (2011), we also applied the letter B (base) in the same meaning of LO, and T (top) in the same meaning of (HO).

In addition, the *Globorotalia menardii* complex abundance events (*G. menardii* zonation) from Ericson and Wollin (1968) were employed and referred to as EW68 zones/subzones. *G. menardii* complex refers to the assemblage which combines *G. menardii* spp., *Globorotalia tumida,* and *Globorotalia flexuosa* without distinction between the different morphotypes or subspecies. The same nomenclature was applied for *Globorotalia crassaformis* (*G. crassaformis*, *G. hessi*, *G. ronda*, *G. viola,* and *G. crassaformis imbricata*) and the *Pulleniatina* (*P. obliquiloculata* and *P. primalis*) genera. However, when the abundance of *G. flexuosa*, *G. crassaformis imbricata*, *G. hessi,* and *G. viola* are considered, their individual relative abundance, rather than those of the complexes are presented. The EW68 zonation is extensively used in biostratigraphic, paleoclimatic and paleoceanographic studies in tropical (e.g., Martin et al., 1990, 1993; Kohl et al., 2004) and subtropical areas (e.g., Vicalvi, 1997; Ferreira et al., 2012, 2014; Portilho-Ramos et al., 2014; Toledo et al., 2016), providing a more detailed biostratigraphic zonation for the Quaternary. For this study, the virtual disappearance of the *G. menardii* complex is defined when its relative abundance drops to <1%. Following Toledo et al. (2016), the disappearance events were numbered top-down by *G. menardii* D1, D2, D3, D4, and D5, and were respectively associated with the base of the EW68 zones Y, W, U, S, and Q. The reappearance events were numbered top-down by *G. menardii* R2, R3, R4, and R5 and were respectively associated with the base of EW68 zones X, V, T, and R.

3.3. Oxygen isotopic analyses and radiocarbon dating

Five specimens of the planktonic foraminifer *Globigerinoides ruber* (white) within the size fraction 250–350 μm, and at least two specimens of the benthic foraminifer *Uvigerina peregrina* and *Cibicidoides wuellerstorfi* within the size fraction >125 μm were hand-picked for stable oxygen isotopic analyses ($\delta^{18}O$). The tests of planktonic foraminifera were soaked in 15% H_2O_2 for 30 min to remove organic matter, and then rinsed with methanol and ultra-sonically cleaned to remove fine-grained particles. The methanol was removed with a syringe, and samples were dried at 50 °C for 24h. The clean foraminifera tests were crushed, and between 20 and 60 mg of calcite was loaded into glass reaction vessels. Benthic foraminifera crushed tests were rinsed with alcohol, dried, and directly loaded into glass reaction vessels. Both planktonic and benthic foraminifera were reacted with three drops of H_3PO_4 (specific gravity = 1.92) using a Finnigan MAT Kiel III carbonate preparation device. Isotope ratios were measured by a Finnigan MAT 252 mass spectrometer. The standard deviation of the international standard NBS19 is < 0.07‰ during the measurement periods. Planktonic foraminifera were analyzed at the Light Stable Isotope Mass Spectrometer Laboratory, Department of Geological Sciences, University of Florida USA. Benthic foraminifera were analyzed at the State Key Laboratory of Marine Geology, Tongji University, China. The results of benthic foraminifera were corrected following Machitto et al. (2014).

Five samples composed of mixed well-preserved specimens of planktonic foraminifera from the size range 250–350 μm were used for radiocarbon (^{14}C) dating (Table 1). The samples were hand-picked and analyzed by accelerator mass spectrometry (AMS) at the National Ocean Sciences Accelerators Mass Spectrometry - USA. The radiocarbon ages were calibrated with the software PaleoDataView version 0.9.2 (Langner and Mulitza, 2019) using the IntCal13 calibration curve (Reimer et al., 2013) and a variable reservoir age correction (Butzin et al., 2017).

The chronology adopted for this study follows Gradstein et al. (2020), where the base of the Quaternary Period, that coincides with the base of the Pleistocene Epoch, has an estimated age of 2.58 Ma. The Pleistocene Epoch is divided into the Gelasian (2.58–1.80 Ma), Calabrian (1.80–0.774 Ma), Middle Pleistocene (Chibanian Stage; 0.774–0.129 Ma) and Upper Pleistocene (0.129–0.011 Ma) (Gibbard and Head, 2020).

4. Results

4.1. Stable oxygen isotopes

The planktonic foraminifera $\delta^{18}O$ values range between −1.64 and 0.38‰ with a maximum amplitude of ~2.02‰ (310 samples; 3210-10 cm core depth; Fig. S2). Lower variability was found near the base of the core (3210 - 2330 cm core depth), with values oscillating between −1.63 and -0.46‰ (average amplitude of −1.03‰; Fig. S2). Above this interval, from 2310 to 1240 cm core depth, the record shows the highest average values −0.63‰, oscillating between-1.41 and 0.38‰, with average amplitude of ~1.79‰. The depth interval 1240-1228 cm showed the highest change between two adjacent samples 2‰ (from 0.38 to −1.62‰; Fig. S2). In the uppermost depth interval 1228-10 cm core depth, the $\delta^{18}O$ values oscillate between-1.64 and 0.02‰ (average amplitude ~1.66‰ and an average value of −0.74‰).

The benthic foraminifera $\delta^{18}O$ record varies from 2.70 to 4.63‰ (average 3.74‰), with a maximum amplitude of ~1.93‰ (288 samples; 3210 - 40 cm core depth; Fig. S2). The lowest variability (amplitude average of ~1.27‰) was found in the base of core (3210 - 2330 cm), with values oscillating between 2.93 and 4.20‰ (mean value of 3.64‰; Fig. S2). Above this interval, from 2310 to 1236 cm core depth, the record shows average values of 3.81‰ (ranging from 2.70 to 4.63‰), with an average amplitude of ~1.93‰. In the uppermost depth interval, 1228 - 40 cm core depth, the $\delta^{18}O$ values oscillate between 2.85 and 4.52‰ (average amplitude~1.67‰ and the average value of 3.87‰).

4.2. Chronology and age model

The age model for core CDH-79 is based on five calibrated AMS ^{14}C ages (Table 1) and 118 $\delta^{18}O$ tie-points (Table S3). The tie-points were derived from the alignment of our $\delta^{18}O$ records to the reference $\delta^{18}O$ stack LR04 (Lisiecki and Raymo, 2005). Following Govin et al. (2015),

Table 1
Raw AMS-^{14}C data and calibrated ages for core CDH-79.

Depth	Lab	Radiocarbon age	Age error	Reservoir age	Reservoir age error	Calibrated age median [95%]	Calibrated age min [95%]	Calibrated age max [95%]
(cm)	ID	(yr BP)	(yr)	(yr)	(yr)	(cal BP)	(cal BP)	(cal BP)
10	OS122410	13900	290	559	55	16054	15225	16942
20	OS122411	17950	510	675	46	20930	19738	22202
30	OS122412	22800	940	781	62	26347	24438	28115
40	OS122413	22900	960	793	63	26437	24506	28272
50	OS122414	25700	1400	740	92	29355	26973	32361

we estimated the age uncertainty for each tie-point (Table S3) by taking into account (i) the mean resolution and dating uncertainty of the reference curve LR04 (resolution 1 ka; uncertainty 6 ka from 2 to 1 Ma and 4 ka from 1 to 0 Ma; Lisiecki and Raymo, 2005), and (ii) an estimated relative alignment uncertainty (~1.04 ka).

The age model and associated uncertainties were calculated by using the BACON algorithm version 2.2 (Blaauw and Christen, 2011) within the PaleoDataView software version 0.9.2 (Langner and Mulitza, 2019). A total of 10,000 age depth realizations have been used to calculate the median age and the 2σ uncertainty at 1 cm resolution for the interval 10–50 cm core depth (Fig. 2b), and 5 cm resolution for the interval 60–3212 cm (Fig. 2a). We assume the presence of a depositional unconformity (hiatus) between 50 and 60 cm, as discussed in section 4.4.

The biochronostatrigraphic model built for core CDH-79 indicates an average accumulation rate of 3.35 cm/ka, showing a good correlation with the LR04 stack (Lisiecki and Raymo, 2005) and the revised isotopic stratigraphies of ODP Leg 154 (Ceara Rise - Sites 925, 927, and benthic smooth; Wilkens et al., 2017), and ODP Site 806b (equatorial Pacific; de Garidel-Thoron et al., 2005) (Fig. 3). CDH-79 reaches an estimated age of 1.93 Ma at the base (i.e., 3212 cm core depth) of the core and records marine isotopes stages (MIS) 1–73, thus continuously covering most of the Quaternary (Fig. 3).

4.3. Planktonic foraminifera and biostratigraphy

A total of 111,749 foraminifera (planktonic and benthic forms) were recovered, of which 99.24% (110,913 specimens) are planktonic forms. In general, the foraminifera presented an excellent state of preservation, which allowed the classification at the species level. Among the 24 recovered species (a taxonomic list is presented at Tables S2) and 14 can be used for the biostratigraphic approach, resulting in the recognition of 19 biostratigraphic events (see details in the supplementary material section Text S1) in the Quaternary of the Pará-Maranhão Basin (Table 2). The events range from the Gelasian to the Upper Pleistocene, with estimated ages of ~1.93 and 0.016 Ma (MIS 73 and MIS 2, respectively).

The LO of *Globorotalia truncatulinodes* (~1.90 Ma; MIS 73), *G. hessi* (~0.78 Ma; MIS 19), and *Globigerinella calida calida* (~0.140 Ma; MIS 6), as well as the HO of *Globigerinoidesella fistulosa* (~1.82 Ma; MIS 66), *Globigerinoides extremus* (~1.77 Ma; MIS 63), *Globigerinoides obliquus* (~1.48 Ma; MIS 49), *Globorotalia tosaensis* (~1.05 Ma; MIS 30/31), and *G. flexuosa* (~0.85 Ma; MIS 5) were used as the main bioevents for the establishment of the biostratigraphy of the area (Table 2; Fig. 4a and b). Also, the relative abundance of the complexes of *G. menardii*, *Pulleniatina*, and *Globorotalia crassaformis*), together with the relative abundance of the species *G. truncatulinoides* and *Globoconella inflata*, were used to define the EW68 zones/subzones.

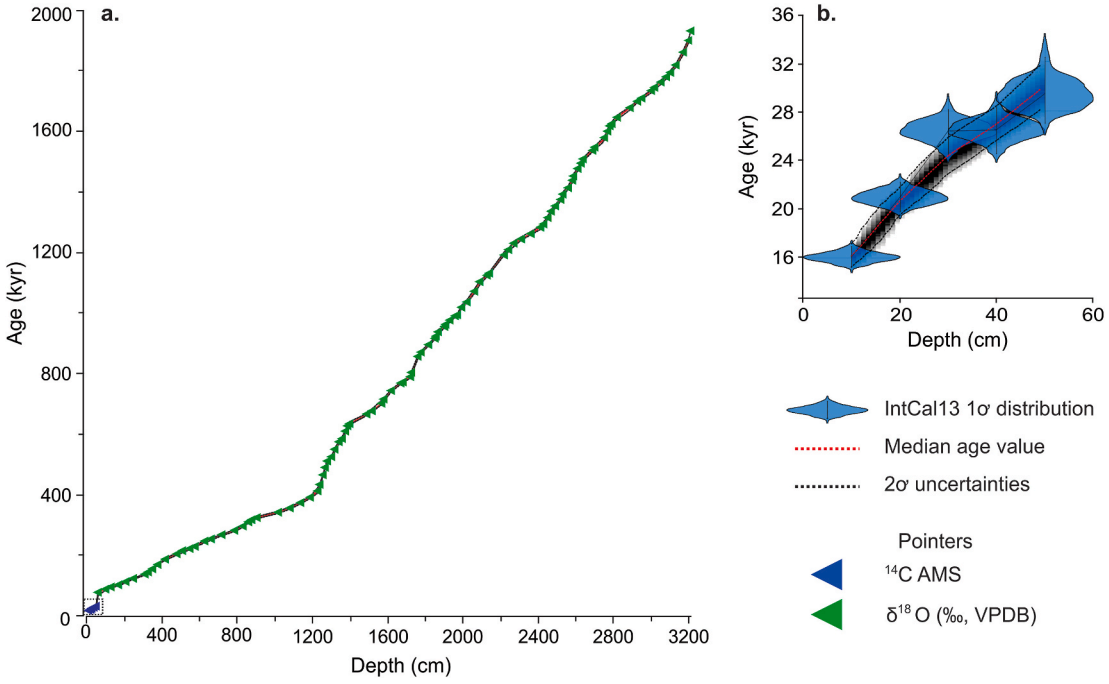

Fig. 2. Age model of core CDH-79 based on calibrated AMS-^{14}C ages (blue triangles) and tie-points (green triangles) based on the alignment of our stable oxygen isotopic ($\delta^{18}O$) records to the reference $\delta^{18}O$ stack LR04 (Lisiecki and Raymo, 2005). Black dotted lines indicate the uncertainty of the median age (solid red line) at (a.) 5 cm, and (b.) 1 cm resolution. Note that between 50 and 60 cm core depth, there is a hiatus. (For interpretation of the references to color in this figure legend, the reader is referred to the Web version of this article.)

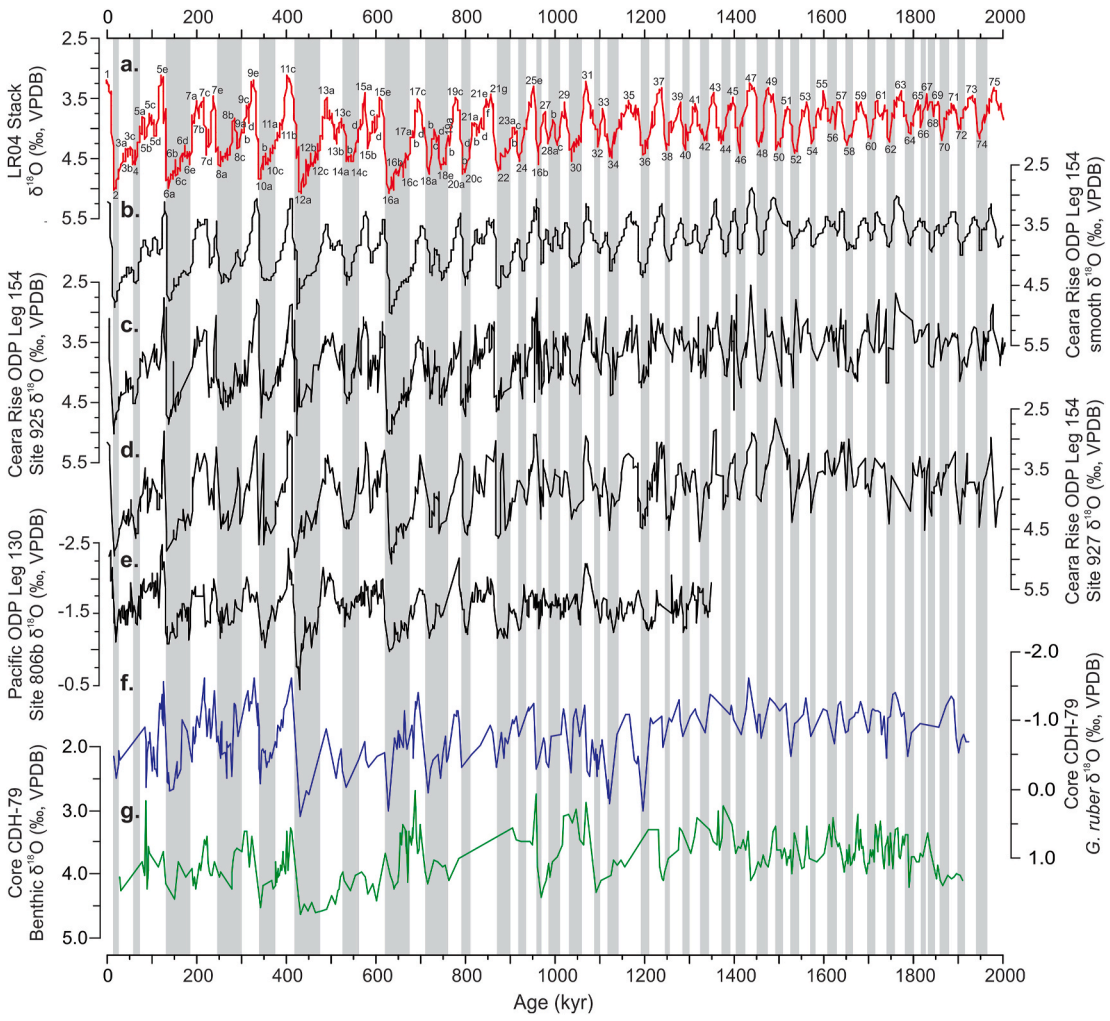

Fig. 3. Stable oxygen isotopic ($\delta^{18}O$) records from (a.) LR04 stack (Lisiecki and Raymo, 2005); revised isotope stratigraphy of Ceara Rise ODP Leg 154 (b.) smooth; (c.) Site 925; (d.) Site 927 (Wilkens et al., 2017); (e) equatorial Pacific ODP Leg 130 - Site 806b (de Garidel-Thoron et al., 2005); and western equatorial Atlantic core CDH-79 (f.) *Globigerinoides ruber* (white); (g.) benthic foraminifera (this study). Marine isotopic stages according to the LR04 stack (Lisiecki and Raymo, 2005), and substages according to Railsback et al. (2015).

The bioevents include *G. menardii* D5 (3092 cm; MIS 63/64; ~1.79 Ma), R5 (2892 cm; MIS 59; ~1.68 Ma), D4 (2032 cm; MIS 30; ~1.05 Ma), R4 (1912 cm, MIS 26/27, ~0.96 Ma), D3 (1362 cm, MIS 15, ~0.59 Ma), R3 (1310 cm; MIS 13/14; ~0.54 Ma), D2 (352 cm, MIS 6, ~0.16 Ma), R2 (292 cm, MIS 5/6; ~0.14 Ma) and D1 (62 cm; MIS 5; ~0.08 Ma) and respectively mark the base of EW68 zones Q, R, S, T, U, V, W, X and Y (Fig. 4a and b; Table 2). The oscillations in abundance are controlled by the entire genus *Pulleniatina,* the *G. crassaformis* complex, as well as the *G. truncatulinoides* and *G. inflata* species, which allowed the division of recognized zones into 20 subzones (Q2, Q1, R3, R2, R1, S2, S1, T4, T3, T2, T1, V3, V2, V1, W2, W1, X3, X2, X1 e Y1A; Fig. 4a and b; Table 3) with a subzonal average resolution of ~85 ka. The detailed descriptions of the EW68 zones and subzones are presented in the supplementary materials (see details in the supplementary material section Text S2).

4.4. Unconformity (hiatus)

Based on the combination of the radiocarbon ages, biostratigraphic events, and MIS identification, two unconformities were detected and confirmed by examination of the core lithology. The lower unconformity was recorded within the interval 60-50 cm core depth (Fig. 5), above the HO of *G. flexuosa* (~0.085 Ma; 70 cm) and *G. menardii* D1 event (~0.08 Ma; 62 cm), both recorded during MIS 5 within EW68 Zone X (Subzone X1), and below the AMS ^{14}C age (Table 1) obtained at 50 cm core depth (~0.03 Ma; MIS 2; EW68 Zone Y). In the visual core description, a thin bed (~2 cm) of sand was observed within the interval 60-50 cm, while the planktonic foraminifera fragmentation rate showed a slight increase. Thus, we suggest the presence of a stratigraphic unconformity (hiatus) close to the top of core CDH-79. This unconformity spans from the top of MIS 5 (~0.08 Ma based on *G. menardii* D1 event) to the base of MIS 2 (~0.03 Ma based on a calibrated AMS ^{14}C age) and is represented by a no depositional/erosional gap covering MIS 4–3 (approximately 50 ka).

The interval 50-10 cm contains no specimens of the *G. menardii* complex. The *G. menardii* R1 event (~0.012 Ma) of Toledo et al. (2016) represents the return of the *G. menardii* complex to the South Atlantic after a period of absence represented by the EW68 Zone Y. Event R1 records Holocene ages and establishes the base of EW68 Zone Z (Holocene) in the Gulf of Mexico and the tropical Atlantic (e.g., Ericson and Wollin, 1968; Martin et al., 1990, 1993; Kohl et al., 2004), as well as the southeastern Brazilian continental margin (e.g., Vicalvi, 1997; Ferreira et al., 2012; Portilho-Ramos et al., 2014; Toledo et al., 2016). The absence of specimens from the *G. menardii* complex in the uppermost samples of core CDH-79 suggests the absence of the EW68 Zone Z and therefore sediments of Holocene age. This topmost hiatus is also supported by the only AMS ^{14}C results of CDH-79 obtained from the interval 10–12 cm (~0.016 Ma; Table 1).

Table 2
Quaternary planktonic foraminifera events ages and marine isotopic stages (MIS) for core CDH-79 and references. The *Globorotalia crassaformis* events as *G. crassaformis* Optimum Event (*Gc*OE) from Portilho-Ramos et al. (2014); and the Highest Common Occurrence (HCO) *G. crassaformis,* the Transition Event (*Gc*TE) and Lowest Common Occurrence (LCO) *G. crassaformis* from Toledo et al. (2016) were also presented; The Quaternary planktonic foraminifera events recorded in the core CDH-79 are highlighted in bold, while the events not recorded are identified by (**).

Bioevents (Datum)	CDH-79		Age - Referecens			Location	References
	Depth (cm)	Age (Ma) (interval)	MIS	(Ma)	MIS		
B *Globorotalia truncatulinoides*				2.58		South Pacific	Srinivasan and Sinha (1992)
				1.93		Ceara Rise	Chaisson and Pearson (1997); Lourens et al. (2004)
				1.93		Revision	Wade et al. (2011)
	3200	**1.90** (1.89–1.91)	**72**			**Pará-Maranhão Basin**	**This work**
T *Globigerinoidesella fistulosa*				1.77		Panama Basin	Shackleton et al. (1990)
				1.88		Ceara Rise	Chaisson and Pearson (1997); Lourens et al. (2004)
	3130	**1.82** (1.81–1.82)	**66**			**Pará-Maranhão Basin**	**This work**
Globorotalia menardii **D5**				1.80		Gulf of Mexico	Martin et al. (1990, 1993)
Base EW68 Zone **Q**	**3092**	**1.79** (1.78–1.79)	**64**			**Pará-Maranhão Basin**	**This work**
T *Globigerinoides extremus*				1.99		Revision	Wade et al. (2011)
				1.98		Ceara Rise	Chaisson and Pearson (1997); Lourens et al. (2004)
				1.80		Lau Basin and Tonga Platform	Chaproniere et al. (1994)
				1.77		Revision	Berggren et al. (1985b); Berggren et al. (1995b)
	3070	**1.77** (1.77–1.78)	**63**			**Pará-Maranhão Basin**	**This work**
Globorotalia menardii **R5**				1.50		Gulf of Mexico	Martin et al. (1990, 1993)
BaseEW68 Zone **R**	**2890**	**1.68** (1.67–1.68)	**59**			**Pará-Maranhão Basin**	**This work**
T *Globigerinoides obliquus*				1.30		Ceara Rise	Chaisson and Pearson (1997); Lourens et al. (2004)
				1.30		Revision	Wade et al. (2011)
	2610	**1.48** (1.47–1.48)	**49**			**Pará-Maranhão Basin**	**This work**
T *Globorotalia tosaensis*				0.61			Mix et al. (1995); Lourens et al. (2004)
	2052	**1.07** (1.06–1.07)	**31**			**Pará-Maranhão Basin**	**This work**
Globorotalia menardii **D4**				1.20		Gulf of Mexico	Martin et al. (1990, 1993)
Base EW68 Zone **S**	**2032**	**1.05** (1.04–1.06)	**30**			**Pará-Maranhão Basin**	**This work**
Globorotalia menardii **R4**				1.00	24/25	Gulf of Mexico	Martin et al. (1990, 1993)
Base EW68 Zone **T**				0.99	27/28		Nishi et al. (2000)
	1912	**0.96** (0.96–0.97)	**26**			**Pará-Maranhão Basin**	**This work**

Table 2. **Continued**

B *Globorotalia hessi*				0.75		Equatorial to Subarctic regions	Bylinskaya (2005)
				0.75	17	Lau Basin and Tonga Platform/Revision	Chaproniere et al. (1994)/Wade et al. (2011)
				0.77		Santos Basin	Toledo et al. (2016)
	1692	**0.78** (0.77–0.78)	**19**			**Pará-Maranhão Basin**	**This work**
Globorotalia menardii **D3**				0.62–0.52	16	Gulf of Mexico	Martin et al. (1993)
Base EW68 Zone **U**				0.61		Gulf of Mexico/Santos Basin	Kohl et al. (2004)/Ferreira et al. (2012)
				0.63	16	Santos Basin	Toledo et al. (2016)
	1362	**0.59** (0.58–0.59)	**15**			**Pará-Maranhão Basin**	**This work**
Globorotalia menardii **R3**				0.48		Gulf of Mexico/Santos Basin	Kohl et al. (2004)/Ferreira et al. (2012)
Base EW68 Zone **V**					13	Caribbean Sea	Martin et al. (1990); Martinez et al. (2007)
				0.49	13	Santos Basin	Toledo et al. (2016)
	1312	**0.54** (0.53–0.55)	**13/14**			**Pará-Maranhão Basin**	**This work**
				1.47		Rio Grande Rise	Barash and Oskina, 1983
T *Globorotalia viola*				1.48			Bylinskaya (2005)
	1040	**0.34** (0.34–0.51)	**10**			**Pará-Maranhão Basin**	**This work**
T *Globorotalia hessi*				0.10–0.20		Equatorial to Subarctic regions	Bylinskaya (2005)
				0.058	4	Santos Basin	Toledo et al. (2016)
	920	**0.33** (0.32–0.33)	**9/10**			**Pará-Maranhão Basin**	**This work**
Globorotalia menardii **D2**				0.20–0.18	7	Gulf of Mexico	Martin et al. (1993)/Kohl et al. (2004)
Base EW68 Zone **W**					7/6	Caribbean Sea	Martin et al. (1990)
					6	Caribbean Sea	Martinez et al. (2007)
				0.142	6b	Santos Basin	Toledo et al. (2016)
	352	**0.16** (0.15–0.16)	**8**			**Pará-Maranhão Basin**	**This work**
B *Globigerinella calida calida*				4.70		Revision	Kennett and Srinivasan (1983)
				0.220		Pacific Ocean	Chaproniere et al. (1994); Wade et al. (2011)
				0.140		Equatorial Atlantic	Bolli and Premoli Silva (1973)
				0.135	6a	Santos Basin	Toledo et al. (2016)

(*continued on next page*)

Table 2 (*continued*)

Bioevents (Datum)	CDH-79		Age - Referecens			Location	References
	Depth (cm)	Age (Ma) (interval)	MIS	(Ma)	MIS		
	320	**0.14** (0.14–0.15)	**6**			**Pará-Maranhão Basin**	**This work**
Table 2. **Continued**							
Globorotalia menardii **R2** Base EW68 Zone **X**				0.13		Gulf of Mexico	Kohl et al. (2004); Martinez et al. (2007)
				0.12	5	Santos Basin	Toledo et al. (2016)
				0.12		Campos Basin	Vicalvi (1997)
	290	**0.13** (0.13–0.14)	**5/6**			**Pará-Maranhão Basin**	**This work**
T *Globorotalia flexuosa*				0.068		Florida Continental slope	Joyce et al. (1990)
				0.084		Santos Basin	Vicalvi (1997), Ferreira et al. (2012)
				0.077		Revision	Berrgren et al. (1995a, b)/Wade et al. (2011)
				0.088	5	Santos Basin	Toledo et al. (2016)
	70	**0.085** (0.080–0.085)	**5**			**Pará-Maranhão Basin**	**This work**
Globorotalia menardii **D1** Base EW68 Zone **Y**				0.090/0.084		Gulf of Mexico	Martin et al. (1993)/Kohl et al. (2004)
				0.084		Campos Basin	Vicalvi (1997); Portilho Ramos et al. (2006)
				0.084		Santos Basin	Ferreira et al. (2012); Toledo et al. (2016)
	62	**0.077** (0.069–0.083)	**5**			**Pará-Maranhão Basin**	**This work**
G. crassaformis Optimum Event *Gc*OE	**	**	**	0.084–0.071		Campos Basin/Santos Basin	Portilho-Ramos et al. (2014)
HCO *G. crassaformis*	**	**	**	0.082.9	5	Santos Basin	Toledo et al. (2016)
G. crassaformis Transition Event *Gc*TE	**	**	**	0.072	5/4	Santos Basin	Toledo et al. (2016)
LCO *G. crassaformis*	**	**	**	0.068.8	4	Santos Basin	Toledo et al. (2016)
*Globorotalia menardii **R1***	**	**	**	0.012		Gulf of Mexico	Kohl et al. (2004)
Base EW68 Zone Z				0.012		Campos Basin	Vicalvi (1997); Portilho Ramos et al. (2006)
B *Globorotalia fimbriata*						Santos Basin	Ferreira et al. (2012); Toledo et al. (2016)
	**	**	**	0.011		Equatorial Atlantic	Bolli and Premoli Silva (1973)

5. Discussion

5.1. Biochronostratigraphic zonation of the western equatorial Atlantic for the last 1.93 Ma

Our data allow the establishment of a biochronostratigraphic framework for the longest Quaternary sediment core from the Pará-Maranhão Basin in the western equatorial Atlantic, spanning from the Gelasian (~1.93 Ma; MIS 73) to the Upper Pleistocene (~0.016 Ma; MIS 2). The evolutionary events allowed the recognition and chronostratigraphic position of the Neogene zones N21 to N22 from Blow (1969), as well as the Cenozoic Zone PL6 and Zone PT1, and the subzones PT1a and PT1b from Berggren et al. (1995a, 1995b) and Wade et al. (2011). The Bolli and Saunders (1985) zones *G. tosaensis tosaensis* and *G. truncatulinoides truncatulinoides* and the subzones *G. crassaformis viola*, *G. crassaformis hessi*, *G. calida calida*, and *G. bermudezi* were further recorded. Appling the EW68 zonation increased the resolution in our record, with ten zones (from P to Y) and 20 subzones, with the first record and description of the zones P, Q, R, and S for the western equatorial Atlantic.

The described stratigraphic unconformities (hiatus; section 4.4) could have been triggered by at least two processes: (i) major changes in sea level at the EW68 zonal boundary X/Y (from the exceptionally warm interglacial MIS 5 to the succeeding glacial MIS 4) and later to the Last Glacial Maximum (Grant et al., 2012) may have triggered mass transport deposits (Martin et al., 1993); or (ii) piston coring may have disturbed the uppermost soft sediments of the sedimentary column (Stow and Aksu, 1978).

5.1.1. Gelasian - Calabrian (~1.93–0.781 Ma – MIS 73–19)

The presence of the *G. menardii* complex at the base of the core (between ~5 and 12%; 3212 - 3102 cm; Fig. 4b), followed by the first disappearance event *G. menardii* D5 (~1.79 Ma; MIS 64; Table 2), support the EW68 Zone P as recorded in the Northwest Gulf of Mexico (ODP 625B), Caribbean Sea (DSDP 502B), and Tropical Atlantic (V16-205) by Martin et al. (1990, 1993). Both presence and disappearance events are recorded for the first time in the western equatorial Atlantic, and Brazilian basins as well. Within Zone P, two evolutionary events have been used to define zone and subzone boundaries, the LO of *G. truncatulinoides,* and HO of *G. fistulosa* (B *G. truncatulinoides*, ~1.90 Ma; T *G. fistulosa*, ~1.82 Ma; Table 2). The absence of *G. truncatulinoides* associated with the presence of *G. tosaensis* recorded between the base of core CDH-79 and the LO of *G. truncatulinoides* (3200 cm, MIS 72; Table 2) points towards the Neogene Zone N21 of Blow (1969). Bolli and Saunders (1985) associated the upper part of Blow's Zone N21 with the Zone *G. tosaensis tosaensis* (Bolli and Premoli Silva, 1973), as recorded in core CDH-79. The LO of *G. truncatulinoides* has been used to define the boundary of the Neogene zones N21/N22 (Blow, 1969), and between the Bolli and Saunders (1985) Zone *G. tosaensis tosaensis* and Quaternary Zone *G. truncatulinoides truncatulinoides* as well. The HO of *G. fistulosa* (3130 cm, MIS 66; Table 2) defined the boundary between the basal Zone PL6 – *Globigerinoides fistulosa* Highest-occurrence Zone and Zone PT1 – *Globigerinoides ruber* Partial-range Zone, and the boundary between Zone PL6 and Subzone PT1a - *Globorotalia tosaensis* Highest-occurrence Subzone as well (Berggren et al., 1995a, 1995b; Wade et al., 2011). The evolutionary events place the base of the core in the Neogene Zone N21 (Blow, 1969), and in the Cenozoic Zones PL6 (Berggren et al., 1995a, b; Wade et al., 2011) and *G. tosaensis tosaensis* (Bolli and Saunders, 1985), while the abundance event *G. menardii* D5

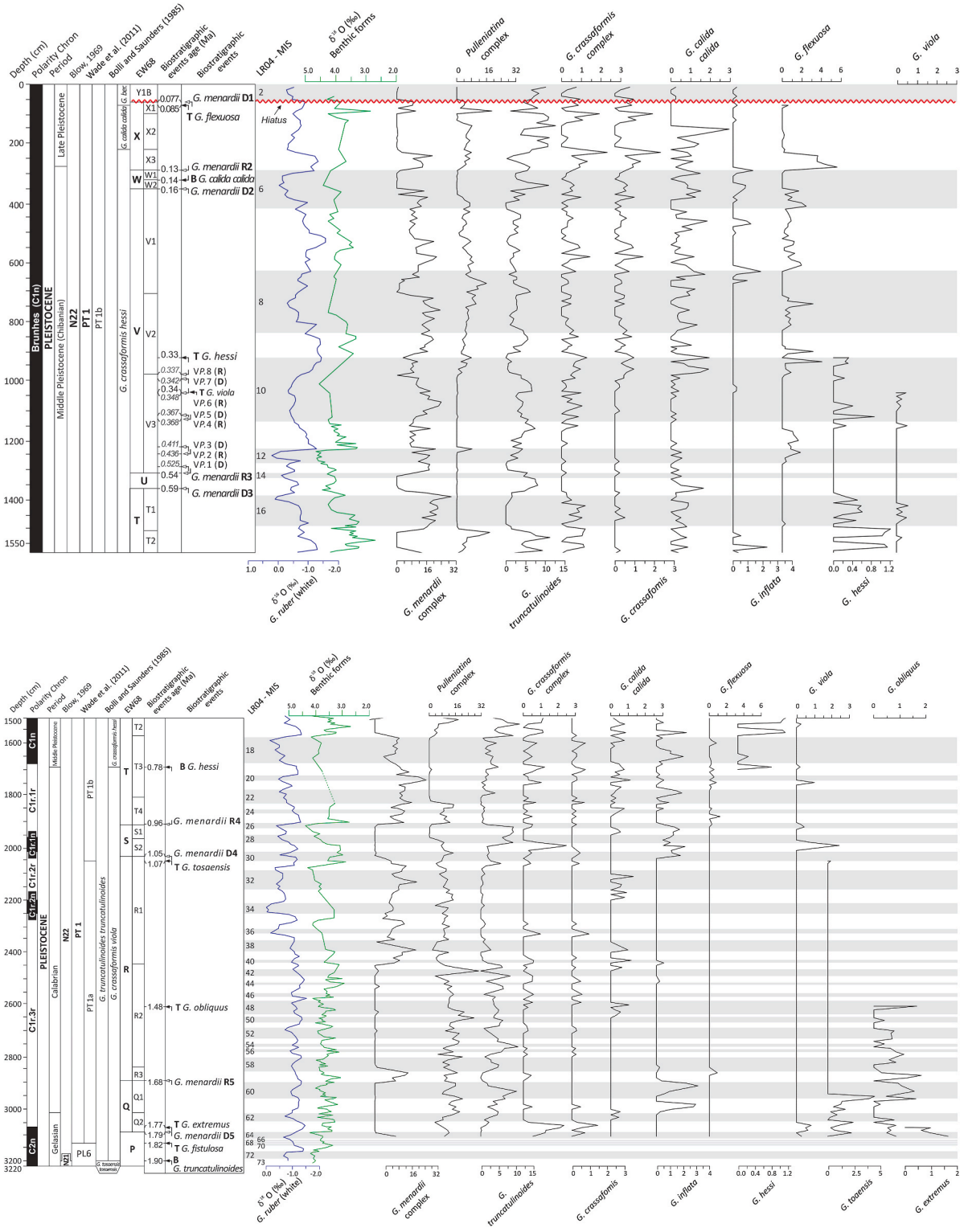

Fig. 4. a. Planktonic foraminifera biostratigraphy of core CDH-79. Quaternary Polarity time scale (C1n = Brunhes; C1r.1r = Matuyama; C1r.1n = Jaramillo; C1r.2n = Cobb Mountain; C2n = Olduvai) of Ogg (2020); Zonal scheme (EW68 = Ericson and Wollin, 1968; Subzone *G. ber.* = *G. bermudezi* Subzone), biostratigraphic events (*V.P.* = *Pulleniatina* complex events - see Table 4; T = top/highest occurrences, B = base/lowest occurrence; D = disappearance, R = reappearance) and estimated ages; planktonic (blue) and benthic (green) oxygen isotopic records ($\delta^{18}O$) and LR04 marine isotope stages (MIS; numbered gray and white horizontal bands; Lisiecki and Raymo, 2005); and relative abundance of selected planktonic foraminifera species.

Fig. 4b. Planktonic foraminifera biostratigraphy of core CDH-79. Quaternary Polarity time scale (C1n = Brunhes; C1r.1r = Matuyama; C1r.1n = Jaramillo; C1r.2n = Cobb Mountain; C2n = Olduvai) of Ogg (2020); Zonal scheme (EW68 = Ericson and Wollin, 1968), biostratigraphic events (T = top/highest occurrences, B = base/lowest occurrence; D = disappearance, R = reappearance) and estimated ages; planktonic (blue) and benthic (green) oxygen isotopic records ($\delta^{18}O$) and LR04 marine isotope stages (MIS; numbered gray and white horizontal bands; Lisiecki and Raymo, 2005); and relative abundance of selected planktonic foraminifera species. . (For interpretation of the references to color in this figure legend, the reader is referred to the Web version of this article.)

Table 3
Ericson and Wollin (1968) zones and subzones, calibrated ages, marine isotope stages (MIS), and accumulation rate in core CDH-79. The disappearance events of *G. menardii* complex were associated with the base of the EW68 zones Y, W, U, S, and Q, while the reappearance events were associated with the base of the zones X, V, T, and R. The MIS identifications were based on the reference $\delta^{18}O$ stack LR04 (Lisiecki and Raymo, 2005).

EW68		Depth(cm)		Age (Ma)		MIS (LR04)		Accumulation
Zones	/Subzones	Top	Base	Top	Base	Top	Base	rate (cm/ka)
Y		10	52	0.02	0.03	2	2	3.18
X	**X1**	60	92	0.08	0.09	5	5	3.28
	X2	100	222	0.09	0.12	5	5	4.66
	X3	230	292	0.12	0.13	5	5/6	4.11
W	**W1**	300	322	0.13	0.14	6	6	2.87
	W2	330	352	0.15	0.16	6	6	2.12
V	**V1**	360	702	0.16	0.26	6	8	3.34
	V2	710	982	0.26	0.34	8	9	3.75
	V3	990	1312	0.34	0.54	9	13/14	1.60
U		1320	1362	0.55	0.59	14	15	1.06
T	**T1**	1370	1500	0.60	0.67	15	16	1.85
	T2	1510	1562	0.68	0.70	16	17	2.19
	T3	1570	1802	0.70	0.89	17	22	1.27
	T4	1810	1912	0.89	0.96	22	26	1.41
S	**S1**	1920	1962	0.97	0.99	26/27	28	1.92
	S2	1970	2032	1.00	1.05	28	30	1.18
R	**R1**	2040	2442	1.06	1.31	30/31	41	1.60
	R2	2450	2832	1.32	1.65	41	58	1.13
	R3	2840	2892	1.66	1.68	58	59	2.41
Q	**Q1**	2900	3002	1.68	1.74	59	61	1.97
	Q2	3010	3092	1.74	1.79	61	64	1.67
P		3102	3212	1.80	1.93	64	73	0.94

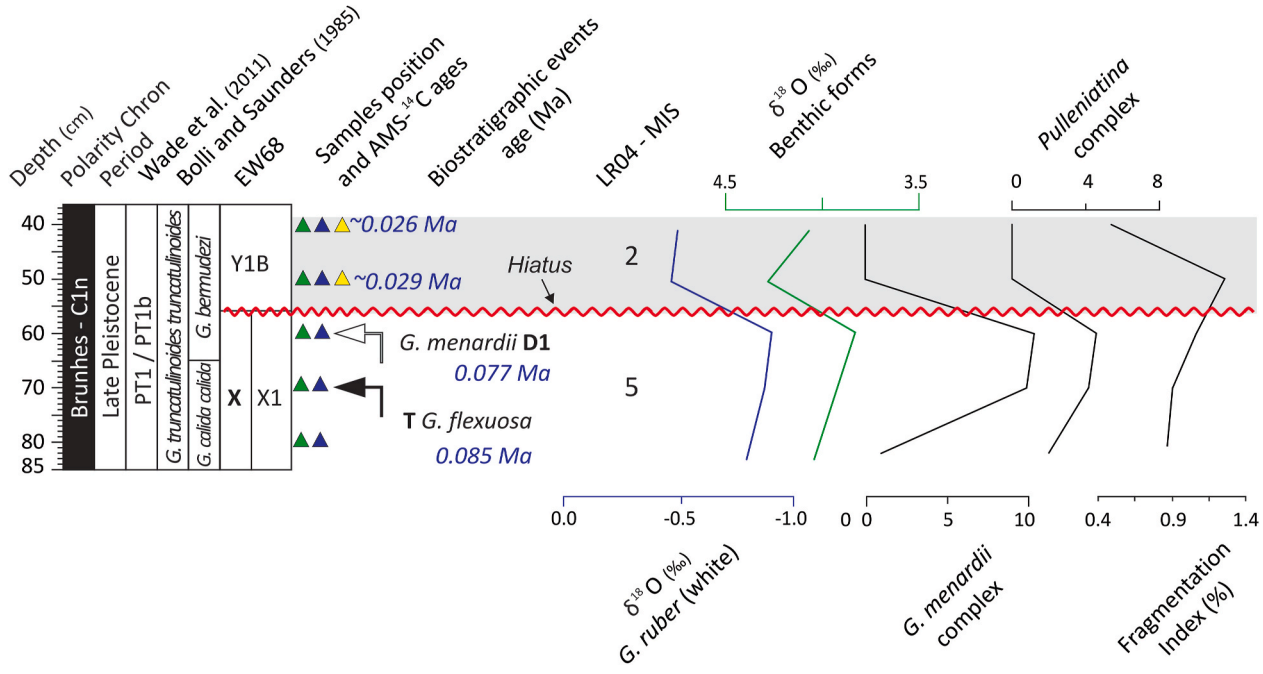

Fig. 5. Position of the lower unconformity recorded between 60 and 50 cm of core CDH-79. Quaternary polarity time scale (Ogg, 2020); Planktonic foraminifera zonal scheme (EW68 = Ericson and Wollin, 1968); location of samples used for planktonic foraminifera biostratigraphic events and estimated ages (green triangles; T = top/highest occurrence, D = disappearance), oxygen isotopic records ($\delta^{18}O$; blue triangles), AMS-^{14}C analyses (yellow triangles; the values denote calibrated AMS ^{14}C ages); LR04 marine isotope stages (MIS; numbered gray and white horizontal bands; Lisiecki and Raymo, 2005), and planktonic (blue) and benthic (green) oxygen isotopic records ($\delta^{18}O$); and relative abundance of *G. menardii* and *Pulleniatina* complexes; and Fragmentation index. (For interpretation of the references to color in this figure legend, the reader is referred to the Web version of this article.)

position it in EW68 Zone P. Taken together, we place the base of core CDH-79 within the Olduvai Subchron (C2n) supporting an estimated age between 1.90 and 1.93 Ma (median age 1.92 Ma; MIS 73), as indicated by our $\delta^{18}O$ records (Figs. 2 and 3).

The LO of *G. truncatulinoides* is recorded for the first time in the Pará-Maranhão Basin, supporting the position of both zones, Blow (1969) Neogene Zone N22, and Quaternary Zone *G. truncatulinoides* of Bolli and Saunders (1985) on the interval 3200 - 10 cm of the core CDH-79. The HO of *G. fistulosa* marks the base of Zone PT1, which extends from the HO of *G. fistulosa* to the Recent, further characterized by the base of Subzone PT1a, which ranges the HO of *G. fistulosa* to the HO of *G. tosaensis* (Berggren et al., 1995a, b; Wade et al., 2011). These events differ slightly in chronostratigraphic position from the ages reported in the literature (e.g., Shackleton et al., 1990;

Srinivasan and Sinha, 1992, Table 2). However, in the tropical Atlantic (Site 925; Chaisson and Pearson, 1997) they appeared isochronously (e.g., Lourens et al., 2004; Wade et al., 2011). An exception occurs with the event HO of *G. tosaensis* (usually record above the HO of *G. hessi,* Wade et al., 2011), which is located earlier in CDH-79 within MIS 31 (2050 cm; Table 2). This inserts the top of Subzone PT1a, as well as the subzonal boundary PT1b/PT1a, within the Calabrian in the Pará-Maranhão Basin (between 1.06 and 1.07 Ma).

The evolutionary HO events of *G. extremus* (T *G. extremus* – median age 1.77 Ma; MIS 63) and *G. obliquus* (T *G. obliquus* - 1.48 Ma; MIS 49), are in accordance with a Calabrian age (older than ~1.40 Ma) for the interval below 2610 cm core depth (Table 2; Fig. 4b). The abundance events *G. menardii* R5 (1.78–1.79 Ma, MIS 64), *G. menardii* D4 (1.04–1.06 Ma, MIS 30), and *G. menardii* R4 (0.96–0.97 Ma, MIS 26) mark the base and the first record of EW68 zones R, S, and T, for this area. These *G. menardii* events further support Calabrian ages for the interval 2890 - 1910 cm core depth (Table 2; Fig. 4b). The event HO of *G. extremus* can be correlated with the top of the Olduvai Subchron (~1.77 Ma; Lourens et al., 2004; Ogg et al., 2020) in our core, and are considered to be isochronous as previously observed in the southwest Pacific (DSDP Legs 22, 23, 24 and 90) by Srinivasan and Shina (1992) and in the Lau Basin (ODP Leg 135, Sites 834, 835, 837, and 839) and Tongan Platform (ODP Leg 135, Sites 840 and 841) by Chaproniere et al. (1994). The events *G. menardii* R5 and HO *G. obliquus* appear older (around 180 ka) than previously published (e.g., Martin et al., 1990, 1993; Wade et al., 2011, Table 2), while *G. menardii* D4 (boundary S/R) and *G. menardii* R4 (boundary T/S) present lower records in the Gulf of Mexico (Martin et al., 1990, 1993, Table 2). In our record, however, the *G. menardii* complex events D4 and R4 showed slight differences in both ages, base (MIS 31; ~1.07 Ma) and top (MIS 28; ~0.99 Ma) of Jaramillo Subchron (C1r.1n). Yet, these abundance events can be used to estimate the position of the Subchron in the Brazilian Equatorial Margin, as diachronism presumably is related to the changes in the climatic system of the Mid-Pleistocene Transition (Berger et al., 1993; Berger and Loutre, 1994). The Mid-Pleistocene Transition marks the change from an earlier 41-ka dominant oscillation to the higher-amplitude100-ka eccentricity-dominated periodicity present in the Upper Pleistocene. These higher amplitude and longer duration glacial/interglacial cycles mark the reorganization of ice sheets and ocean currents around 0.9 Ma (MIS 25–22; Berger et al., 1993; Nishi et al., 2000), which might contribute to higher uncertainties in the transitions of S/R and T/S zones (Caley et al., 2012).

The LO of *G. hessi* (0.77–0.78 Ma; Table 2) occurs within the lower $\delta^{18}O$ values of MIS 19 (Subzone T3) and has been used as a marker for the top of Calabrian Subzone *G. crassaformis viola* (Bolli and Premoli Silva, 1973). The presence of *G. viola* between evolutionary events LO of *G. truncatulinoides* and LO of *G. hessi* (Table 2) supports a Gelasian to Calabrian age, spanning from ~1.93–0.781 Ma (MIS 73–19) and the Subzone *G. crassaformis viola* to this interval. This event is synchronous to the one recorded by Toledo et al. (2016) in the Santos Basin and is used in our records to define the boundary between the Calabrian and the Middle Pleistocene.

5.1.2. *Middle Pleistocene (~0.781–0.126 Ma – MIS19-6)*

The Middle Pleistocene is characterized by the Subzone *G. crassaformis hessi* (Bolli and Premoli Silva, 1973) indicated at the base by the LO of *G. hessi* (B *G. hessi* - 0.78 Ma; MIS 19; Table 2) and at the top by the LO of *G. calida calida* (0.14–0.15 Ma; Table 2). This Subzone covers almost the entire Middle Pleistocene. In addition to these zonal marker events, three abundance events of the *G. menardii* complex (D3, R3, and D2) were recorded within this subzone in the Pará-Maranhão Basin, supporting the Middle Pleistocene age estimate (Fig. 4a and b; Table 2). The evolutionary event HO of *G. hessi* is usually associated with the Subzone *G. calida calida* (Upper Pleistocene), however, this event appears to be older in our record, within Subzone V2 in the Middle Pleistocene, showing a wider range in comparison with the tropical Atlantic (0.20–0.10 Ma; Bylinskaya, 2005) and southeastern Brazilian continental margin (Cores GL-852 and GL-854; Toledo et al., 2016). Besides.

The event *G. menardii* D3 had been recorded in the Santos Basin around 0.63 Ma (MIS 16; Toledo et al., 2016), while in the Gulf of Mexico it was registered at ~0.61 Ma (Kohl et al., 2004) and between 0.62 and 0.52 Ma (MIS 16 - MIS 15; Martin et al., 1990, 1993) suggesting that this event occurred first in the South Atlantic and later in the North Atlantic. In the Pará-Maranhão Basin, the third disappearance of the *G. menardii* complex (*G. menardii* D3; 0.58–0.59 Ma) occurs within a small increase in $\delta^{18}O$ values during MIS 15 (Fig. 4a and b). Our records show a younger age than reported in the North and South Atlantic (Table 2), suggesting that the *G. menardii* complex D3 spread from the South and North Atlantic to the equatorial Atlantic. The third reappearance event of *G. menardii* complex (R3), in turn, occurred first in the equatorial Atlantic, spreading later to the southeastern Brazilian continental margin (Toledo et al., 2016), the Caribbean Sea and North Atlantic (Gulf of Mexico; Martin et al., 1993). This is an opposite trend than that of the *G. menardii* D3.

As described by Ferreira et al. (2012) for the southeastern Brazilian continental margin, a set of disappearance and reappearance events of the *Pulleniatina* complex (Table 4) has been recorded in the base of EW68 Zone V (Subzone V3). In general, these events appear to be older in the southeastern Brazilian continental margin (Cores BS-C and BS-D; Santos Basin), spreading later to the equatorial Atlantic (core CDH-79; Pará-Maranhão Basin). An exception is event V*P*.1, which occurs first in the equatorial margin. Prell and Damuth (1978) in the Gulf of Mexico, the Caribbean Sea, and equatorial Atlantic recorded a set of disappearance and reappearance events of the *Pulleniatina* complex, especially from *Pulleniatina obliquiloculata,* during the last 0.175 Ma (EW68 zones V to Z; Middle Pleistocene to Holocene), named as biohorizon Y*P*. Those authors used these events for regional correlation during EW68 Zone Y. These events presented diachronic ages, ranging from ~0.60 Ma in the Gulf of Mexico to ~0.50 Ma in the Caribbean Sea and ~0.35 Ma in the

Table 4
Position, ages, and marine isotope stages (MIS) of *Pulleniatina* complex disappearance (D) and reappearance (R) events in the Ericson and Wollin (1968) Zone V (Subzone V3) of core CDH-79, western equatorial Atlantic (text in bold; this study). Events ages from the Santos Basin cores BS-C and BS-D, southeastern Brazilian continental margin (normal text), are from Ferreira et al. (2012).

Pulleniatina complex	Zone/	Age (Ma)			MIS	Depth (cm)
events	Subzone	BS-C	BS-D	CDH-79	CDH-79	CDH-79
V*P*.8 **(R)**	V2	0.357	0.379			
	V3			**0.337 (0.332–0.340)**	**9**	**980**
V*P*. 7 **(D)**	V3	0.399	0.400			
	V3			**0.342 (0.338–0.345)**	**10**	**1010**
V*P*. 6 **(R)**	V3	0.410	0.407			
	V3			**0.348 (0.344–0.351)**	**10**	**1040**
V*P*. 5 **(D)**	V3	0.416	0.428			
	V3			**0.367 (0.364–0.372)**	**10**	**1120**
V*P*. 4 **(R)**	V3	0.446	0.450			
	V3			**0.368 (0.364–0.372)**	**10**	**1122**
V*P*. 3 **(D)**	V3	**	0.462			
	V3			**0.411 (0.406–0.422)**	**11**	**1228**
V*P*. 2 **(R)**	V3	**	0.471			
	V3			**0.436 (0.430–0.441)**	**12**	**1242**
V*P*. 1 **(D)**	V3	0.481	0.480			
	V3			**0.525 (0.522–0.530)**	**13**	**1300**

equatorial Atlantic. These events showed older ages in the North Atlantic, and later spread to the equatorial Atlantic (Prell and Damuth, 1978), an opposite behavior from that observed for the proposed events of Zone V in the equatorial Atlantic (Pará-Maranhão Basin). Although the *Pulleniatina* complex disappearance and reappearance events can be established as biostratigraphic markers, their local and regional correlation to the EW68 Zone V needs further investigation.

The diachronism recorded for *G. menardii* D2 event at the base of EW68 Zone W (Subzone W2), supports the conclusion of Toledo et al. (2016) of the disappearance of *G. menardii* complex initially in the Northern Hemisphere, in the Gulf of Mexico and the Caribbean Sea (0.20–0.18 Ma - MIS7/6 to 7; Martin et al., 1993 and Kohl et al., 2004), spreading to the equatorial Atlantic (0.15–0.16 Ma – MIS 6; Table 2), and later to the southeastern Brazilian continental margin (~0.14 Ma – MIS6b; Toledo et al., 2016). Recorded within EW68 Zone W (Subzone W1; Table 2), the LO of *G. calida calida* (~0.14 Ma; MIS 6; Table 2) marks the top of the Bolli and Premoli Silva (1973) Pleistocene Subzone *G. crassaformis hessi*, and upper Middle Pleistocene, close to the boundary between Middle and Upper Pleistocene in our core.

The HO of *G. tosaensis,* recorded during the Lower Pleistocene in the Pará-Maranhão Basin, marks the base of Wade et al. (2011) Subzone PT1b. According to Berggren et al. (1995a, b) and Wade et al. (2011) this Subzone (PT1b) spans the last 0.61 Ma (from 0.61 Ma to the Recent), and support the interval covered by the Bolli and Premoli Silva (1973) Subzone *G. crassaformis hessi* and Subzone *G. calida calida* were represented by sediments deposited during the Middle Pleistocene (between 0.781 and 0.126 Ma).

5.1.3. Late Pleistocene (0.126–0.016 Ma)

The LO of *G. calida calida* marks the boundary between the Middle Pleistocene Subzone *G. crassaformis hessi* and the Bolli and Premoli Silva (1973) Late Pleistocene Subzone *G. calida calida*. This Subzone extends from the LO of *G. calida calida* to the HO of *G. flexuosa* (0.080–0.085 Ma; Table 2). In addition to the zonal markers, one abundance event has been recorded within this Subzone, namely the fourth reappearance event of the *G. menardii* complex (R2). The *G. menardii* R2 event (0.13–0.14 Ma; Table 2) from Toledo et al. (2016), marks the base of the EW68 Zone X. This zone was recorded in many basins from the North and South Atlantic during the last ~0.13 Ma (e.g., Ericson and Wollin, 1968; Martin et al., 1990, 1993; Vicalvi, 1997; Kohl et al., 2004; Ferreira et al., 2012; Portilho-Ramos et al., 2014; Toledo et al., 2016), supporting the suggestion that the interval represents the Late Pleistocene. The HO of *G. flexuosa* has been recorded in the Pará-Maranhão Basin with an estimated median age of 0.085 Ma (Table 2), representing the top of Subzone *G. calida calida*, and the boundary between the subzones *G. calida calida* and *G. bermudezi*, subzone from Bolli and Premoli Silva (1973).

The Late Pleistocene Subzone *G. bermudezi* has been recorded in the top of core CDH-79 (62–0 cm; Fig. 4a). During this Subzone, the abundance *G. menardii* D1 event (0.069–0.083 Ma; Table 2) has been recorded, marking the boundary between EW68 zones X/Y. The records in core CDH-79 suggest the presence of a hiatus (around 50 ka), during the Subzone *G. bermudezi*, located above the *G. menardii* D1 event, and below to the AMS ^{14}C sample at 50 cm (median age 0.030 Ma; Table 1; Fig. 5). The absence of the abundance events based on the *G. crassaformis* complex recorded by Portilho-Ramos et al. (2014) and Toledo et al. (2016) above the *G. menardii* D1 event confirms the presence of a hiatus in core CDH-79. The top of our core has a calibrated AMS ^{14}C age ~0.016 Ma (10 cm; Table 1), within the Subzone *G. bermudezi*. The absence of the evolutionary event LO *G. fimbriata* (~0.011 Ma; Bolli and Premoli Silva, 1973), which characterizes the top of Subzone *G. bermudezi*, as well as the boundary between the subzones *G. bermudezi* and *G. fimbriata* from Bolli and Saunders (1985), explains the complete absence of Subzone *G. fimbriata* from core CDH-79. The absence of Subzone *G. fimbriata* in addition to the calibrated AMS ^{14}C ages supports the lack of Holocene sediments in our core from the Pará-Maranhão Basin.

5.2. Summary of the main biostratigraphic events from Gelasian to Late Pleistocene in the western equatorial Atlantic

During the Gelasian to Late Pleistocene (last 1.93 Ma), six species became extinct (HO), and three species appeared (LO) in the Brazilian Equatorial Margin (Table 2; Fig. 4a and b). Biostratigraphic events of highest occurrence (T *G. fistulosa*; T *G. extremus*; Table 2) observed in the base of our core during the Gelasian - Calabrian (~1.93–1.70 Ma) in agreement with previous findings (e.g., Berggren et al., 1985b, 1995b; Chaisson and Pearson, 1997; Lourens et al., 2004). However, the event T *G. obliquus* occurs earlier in our record (1.47–1.48 Ma) than in previous studies (~1.30 Ma; Chaisson and Pearson, 1997; Wade et al., 2011), while the T *G. tosaensis* (1.06–1.07 Ma) and T *G. hessi* (0.32–0.33 Ma) events occurred with a large age difference between records from the tropical Pacific Site 846 (~0.61 Ma; ODP Leg 138; Mix et al., 1995) and southeastern Brazilian continental margin (~0.58 Ma; Toledo et al., 2016). Most of these HO events were recorded during interglacial MIS or deglaciations (Table 2). The most notable exceptions are the HO of *G. fistulosa*, recorded during the glacial MIS 66, and the HO of *G. hessi*, recorded during the MIS 9/10 glacial inception. The LO biostratigraphic events observed in our record (B *G. truncatulinoides*; B *G. hessi*, and B *G. calida calida*; Table 2), on the other hand, agree with previous observations (e.g., Chaisson and Pearson, 1997; Wade et al., 2011; Toledo et al., 2016). These events were associated with glacials, except for the B *G. hessi* that occurred during MIS 19.

In addition to the LO and HO events, the abundance events of the *G. menardii* complex allowed the recognition of ten EW68 zones (from P to Y). We report the oldest *G. menardii* complex Quaternary abundance events in the Brazilian basins. These events are represented by the disappearance of the complex during *G. menardii* D5 (1.78–1.79 Ma) and D4 (1.04–1.05 Ma), while the reappearance events were recorded as R5 (1.67–1.68 Ma) and R4 (0.96–0.97 Ma). The disappearances events *G. menardii* D5 and D4 took place first in the North Atlantic (Gulf of Mexico; Martin et al., 1990, 1993), spreading transgressively to the equatorial Atlantic. The same behavior was observed with the events *G. menardii* D3 and D2, while *G. menardii* D1 was isochronous throughout (Martin et al., 1993; Kohl et al., 2004; Martinez et al., 2007, Table 2). In contrast, *G. menardii* complex reappearances events occurred first in the equatorial Atlantic, spreading later to the North and South Atlantic.

Our data suggest a small diachronism between the disappearance/reappearance events of the *G. menardii* complex compared to the records of North and South Atlantic. The average difference in the age of the *G. menardii* D events (D5, D4, D3, D2, and D1) between the North Atlantic and the equatorial Atlantic (our core CDH-79) is ~0.067 ± 0.022 Ma, while the difference in the age of the *G. menardii* D events (D3, D2, and D1) between the South Atlantic and the equatorial Atlantic is ~0.022 ± 0.010 Ma. However, the average age differences of the *G. menardii* R (events R5, R4, R3, and R2) events between the North Atlantic and equatorial Atlantic are ~0.065 ± 0.040 Ma, while the average difference in the age of the *G. menardii* R events (R3 and R2) between the South Atlantic and the equatorial Atlantic is ~0.030 ± 0.020 Ma. These systematic differences in age may be related to the mechanism responsible for inter-ocean exchange of surface and central waters from the Indian Ocean to the South Atlantic via the Agulhas leakage (Peter et al., 2004; Caley et al., 2012). Caley et al. (2012) demonstrated that the reseeding of *G. menardii* in the Atlantic over the last 1.35 Ma is related to extreme leakage events, associated with the southward migration of the subtropical front. These conditions produced strong peaks in the accumulation rate of *G. menardii* at ODP Site 1087 (southern Benguela region). On the other hand, periods of reduced Indian-to-Atlantic transfer and northward migration of the subtropical front, are marked by minimum abundance, if not complete absence, of the taxon.

6. Conclusions

Based on the identification of planktonic foraminifera from the ~32 m-long core CDH-79 and the calibration of the biostratigraphic events with oxygen isotope records and radiocarbon ages, a bio-chronostratigraphic framework was established for this, the longest continuous record (~1.93–0.01 Ma) in the Brazilian equatorial margin. We present 17 calibrated biostratigraphic events and their associated uncertainties, providing the first recognition and description of the taxon appearance, such as the earliest presence of *G. truncatulinoides* (1.89–1.91 Ma) and taxon disappearance, such as *G. fistulosa* (1.81–1.82 Ma) for the Pará-Maranhão Basin. Evolutionary events in deeper time, such as last occurrences of *G. fistulosa* and *G. viola* appear to be younger in our record, while *G. obliquus* and *G. tosaensis* presented older ages than in previously published records. The explanation for these differences is not known, demonstrating the need for more biostratigraphic studies for the lower Pleistocene, particularly in the tropical Atlantic.

Oscillations in the abundance of the *G. menardii* complex showed the oldest Pleistocene disappearance and reappearance events of the complex (*G. menardii* D5, R5, D4, and R4) in the western Atlantic and Brazilian basins in this study. These new events allowed the first determination of the biostratigraphic zones P, Q, R and S and subzones Q2, Q1, R3, R2, R1, S2, and S1 in the Brazilian basins, improving the resolution of lower Pleistocene events for the area. Our data presented a small diachronism of *G. menardii* events compared to other sites in the North and South Atlantic, possible related to the reseeding mechanism of the taxon due to latitudinal migration of the subtropical front, which appears to be directly connected to the strength of warm waters entering the South Atlantic from the Indian Ocean through the Agulhas leakage.

The integration of observations of the bioevents *G. menardii* R2 (reappearance) and T *G. flexuosa* (disappearance), a radiocarbon age, and lithologic observation, suggests the presence of an unconformity (hiatus) of approximately 50 ka close to the top of our core (i.e., 50–62 cm core depth) between MIS 5 and MIS 2. Furthermore, the absence of *G. menardii* R1 event and *G. fimbriata* specimens, corroborated by the uppermost radiocarbon age (10 cm core depth), demonstrate the absence of sediments deposited during the Holocene. Both unconformities were recognized in the upper section of our records (uppermost 60 cm) and may relate to changes in sea level and/or coring disturbance.

This record greatly improves the resolution of the biostratigraphic events from the Gelasian to the Late Pleistocene, thus forms an important basis for improved age constraints for all future paleoenvironmental reconstructions in the tropical western Atlantic.

Author contributions

Fabricio Ferreira: Conceptualization; Methodology; Data Curation; Formal analysis; Investigation; Writing - Original Draft. **Cleverson G. Silva:** Resources; Writing - Review & Editing; Supervision; Project administration. **Allan S.Oliveira:** Data Curation; Formal analysis. **Cristiano M. Chiessi:** Writing - Review & Editing. **Andrea K. Kern:** Writing - Review & Editing. **Paul A. Baker:** Resources; Writing - Review & Editing; Supervision; Project administration. **Gary Dwyer:** Writing - Review & Editing. **Catherine A. Rigsby:** Writing - Review & Editing. **Enqing Huang:** Formal analysis. **Jun Tian:** Formal analysis.

Data availability

Datasets related to this article can be found at https://doi.pangaea.de/10.1594/PANGAEA.917897, an open-source online data repository hosted at PANGAEA (Ferreira et al., 2020).

Declaration of competing interest

The authors declare that they have no known competing financial interests or personal relationships that could have appeared to influence the work reported in this paper.

Acknowledgments and Funding

Fabricio Ferreira has the support of the Brazilian agency CAPES [grant numbers 88882.151083/2017–01, and 88881.185132/2018–01], which allowed the development of this study. C. M. Chiessi acknowledges the financial support from FAPESP [grant numbers 2018/15123–4, and 2019/24349–9], CAPES [grant numbers 564/2015 and 88881.313535/2019–01], CNPq [grant numbers 302607/2016–1, and 312458/2020–7] and the State Key Laboratory of Marine Geology, Tongji University, China [grant MGK1602]. A. K. Kern received funding from FAPESP [grant numbers 2014/05582–0, and 2015/18314–7] and CAPES [grant number 88887.370034/2019–00].

Appendix A. Supplementary data

Supplementary data to this article can be found online at https://doi.org/10.1016/j.quaint.2021.04.042.

References

Arz, H.W., Pätzold, J., Wefer, G., 1998. Correlated millennial-scale changes in surface hydrography and terrigenous sediment yield inferred from last-glacial marine deposits off northeastern Brazil. Quat. Res. 50 (2), 157–166.

Arz, H.W., Patzold, J., Wefer, G., 1999. The deglacial history of thewestern tropical Atlantic as inferred from high-resolution stable isotope records off northeastern Brazil. Earth Planet Sci. Lett. 167, 105–117.

Barash, M.S., Oskina, N.S., 1983. Quaternary biostratigraphy and surface paleotemperatures based on planktonic foraminifera. In: Barker, P.F., Carlson, R.L., Johnson, D.A., et al. (Eds.), Init. Repts. DSDP, vol. 72. U.S. Govt. Printing Office), Washington.

Bé, A.W.H., Damuth, J.E., Lott, L., Free, R., 1976. Late quaternary climatic record in western equatorial Atlantic sediment. In: Geological Society of America. Investigations of Late Quaternary Paleoceanography and Paleoclimatology, vol. 145. Geological Society of America Memoir, pp. 162–200.

Berger, W.H., Bickert, T., Schmidt, H., Wefer, G., 1993. Quaternary oxygen isotope record of pelagic foraminifers: site 806, Ontong Java Plateau. In: Berger, W.H., Kroenke, L.W., Mayer, L.A., et al. (Eds.), ODP Proceedings Scientific Results, vol. 130, pp. 381–395. College Station, TX.

Berger, W.H., Loutre, M.F., 1994. Precession, eccentricity, obliquity, insolation and paleoclimates. In: Duplessy, J.-C., Spyridakis, M.T. (Eds.), Long-Term Climatic Variations: Data and Modeling, vol. 22. NATO Science Series, pp. 107–152.

Berggren, W.A., Kent, D.V., van Couvering, J.A., 1985a. Neogene geochronology and chronostratigraphy. In: Snelling, N.J. (Ed.), The Chronology of the Geological Record, vol. 10. Geological Society of London Memoir, pp. 211–250.

Berggren, W.A., Kent, D.V., Flynn, J.J., van Couvering, J.A., 1985b. Cenozoic geochronology. Geol. Soc. Am. Bull. 96, 1407–1418.

Berggren, W.A., Hilgen, F.J., Langereis, C.G., Kent, D.V., Obradovich, J.D., Raffi, I., Raymo, M.E., Shackleton, N.J., 1995a. Late Neogene chronology: new perspectives in high-resolution stratigraphy. Geol. Soc. Am. Bull. 107, 1272–1287.

Berggren, W.A., Kent, D.V., van Couvering, J.A., 1995b. Neogene geochronology and chronostratigraphy. Geological Society Memoirs 10, 211–260. https://doi.org/10.1144/GSL.MEM.1985.010.01.18.

Blaauw, M., Christen, J.A., 2011. Flexible paleoclimate age-depth models using an autoregressive gamma process. Bayesian Analysis 6 (3), 457–474.

Blow, W.H., 1969. Late middle Eocene to Recent planktonic foraminiferal biostratigraphy. In: Bronnimann, P., Renz, H.H. (Eds.), Proceedings of the First International Conference on Planktonic Microfossils, pp. 199–422. Geneva.

Bolli, H.M., Premoli Silva, I., 1973. Oligocene to recent planktonic foraminífera and stratigraphy of Leg 15 sites in the Caribean sea. Initial Rep. Deep Sea Drill. Proj. 15, 475–497.

Bolli, H.M., Saunders, J.B., 1985. Oligocene to Holocene low latitude planktic foraminifera. In: Bolli, H.M., Saunders, J.B., Perch-Nielsen, K. (Eds.), Plankton Stratigraphy. Cambridge University Press, New York, pp. 156–262.

Butzin, M., Köhler, P., Lohmann, G., 2017. Marine radiocarbon reservoir age simulations for the past 50,000 years. Geophys. Res. Lett. 44, 8473–8480. https://doi.org/10.1002/2017GL074688.

Bylinskaya, M.E., 2005. Range and stratigraphic significance of the *Globorotalia crassaformis* plexus. J. Iber. Geol. 31 (1), 51–63.

Caley, T., Giraudeau, J., Malaizé, B., Rossignol, L., Pierre, C., 2012. Agulhas leakage as a key process in the modes of Quaternary climate change. Proc. Natl. Acad. Sci. Unit. States Am. 109 (18), 6835–6839. https://doi.org/10.1073/pnas.1115545109.

Chaisson, W.P., Pearson, P.N., 1997. Planktonic foraminifer biostratigraphy at site 925: middle Miocene-pleistocene. In: Shackleton, N.J., Curry, W.B., Richter, C., Bralower, T.J. (Eds.), Proceedings of the Ocean Drilling Program, Scientific Results, vol. 154.

Chaproniere, G.C.H., Styzen, M.J., Sager, W.W., Nishi, H., Quinterno, P.J., Abrahamsen, N., 1994. Late Neogene biostratigraphic and magnetostratigraphic synthesis, Leg 135. In: Hawkins, J., Parson, L., Allan, J., et al. (Eds.), Proceedings of the Ocean Drilling Program, Scientific Results, vol. 135. Ocean Drilling Program), College Station, TX, pp. 857–877. https://doi.org/10.2973/odp.proc.sr.135.116.1994.

de Garidel-Thoron, T., Rosenthal, Y., Bassinot, F., Beaufort, L., 2005. Stable sea surface temperatures in the western Pacific warm pool over the past 1.75 million years. Nature 433 (7023), 294–298.

Ericson, D.B., Wollin, G., 1968. Pleistocene climates and chronology in deep-sea sediments. Science 162, 1227–1243.

Ferreira, F., Frontalini, F., Leão, C.J., Leipnitz, I.I., 2014. Changes in the water column structure and paleoproductivity in the western South Atlantic Ocean since the middle Pleistocene: evidence from benthic and planktonic foraminífera. Quat. Int. 352, 111–123.

Ferreira, F., Leipnitz, I.I., Vicalvi, M.A., Sanjinés, A.E.S., 2012. Zoneamento Paleoclimático do Quaternário da Bacia de Santos com base em foraminíferos planctônicos. Rev. Bras. Palaontol. 15 (2), 173–188.

Fonseca, C.A., Goni, G.J., Johns, W.E., Campos, E.J.D., 2004. Investigation of the north Brazil current retroflection and north equatorial Countercurrent variability. Geophys. Res. Lett. 31 (21), 1–5. https://doi.org/10.1029/2004GL020054.

Gibbard, P.L., Head, M.J., 2020. Chapter 30 - the Quaternary Period. In: Gradstein, F.M., Ogg, J.G., Schmitz, M.D., Ogg, G.M. (Eds.), Geologic Time Scale 2020. Elsevier, ISBN 9780128243602, pp. 1217–1255. https://doi.org/10.1016/B978-0-12-824360-2.00030-9.

The Subcommission on Quaternary Stratigraphy Gibbard, P.L., Head, M.J., Walker, M.J. C., 2010. Formal ratification of the quaternary system/period and the Pleistocene series/epoch with a base at 2.58 Ma. J. Quat. Sci. 25, 96–102.

Goni, G.J., Johns, W.E., 2001. A census of North Brazil Current Rings observed from TOPEX/POSEIDON altimetry: 1992–1998. Geophys. Res. Lett. 28 (1), 1–4.

Govin, A., Capron, E., Tzedakis, P.C., Verheyden, S., Ghaleb, B., Hillaire-Marcel, C., St-Onge, G., Stoner, J.S., Bassinot, F., Bazin, L., Blunier, T., Combourieu-Nebout, N., El Ouahabi, A., Genty, D., Gersonde, R., Jimenez-Amat, P., Landais, A., Martrat, B., Masson-Delmotte, V., Parrenin, F., Seidenkrantz, M.-S., Veres, D., Waelbroeck, C., Zahn, R., 2015. Sequence of events from the onset to the demise of the Last Interglacial: evaluating strengths and limitations of chronologies used in climatic archives. Quat. Sci. Rev. 129, 1–36.

Gradstein, F.M., Ogg, J.G., Schmitz, M.D., Ogg, G.M., 2020. Geologic Time Scale 2020. Elsevier, iv, ISBN 9780128243602. https://doi.org/10.1016/B978-0-12-824360-2.00033-4.

Grant, K.M., Rohling, E.J., Bar-Mathews, M., Aylon, A., Medina-Elizalde, M., Ramsey, C. B., Satow, C., Roberts, A.P., 2012. Rapid coupling between ice volume and polar temperature over past 150.000 years. Nature 491, 744–747. https://doi.org/10.1038/nature11593.

Haarsma, R.J., Campos, E.J.D., Drijfhout, S., Hazeleger, W., Severijns, C., 2011. Impacts of interruption of the Agulhas leakage on the tropical Atlantic in coupled ocean-atmosphere simulations. Clim. Dynam. 36 (5–6), 989–1003. https://doi.org/10.1007/00382-009-0692-7.

Hayward, B.W., Le Coze, F., Vachard, D., Gross, O., 2019. World foraminifera database. http://www.marinespecies.org/foraminifera on 2019-12-14.

Johns, W.E., Lee, T.N., Beardsley, R., Candela, J., Castro, B., 1998. Annual cycle and variability of the north Brazil current. J. Phys. Oceanogr. 28, 103–128.

Joyce, J.E., Tjalsma, L.R., Prutzman, J.M., 1990. High-resolution planktonic isotope record and spectral analysis for the last 5.35 Ma: ocean drilling program site 625 – northeast Gulf of Mexico. Paleoceanography 5 (4), 507–529.

Kennett, J.P., Srinivasan, M.S., 1983. Neogene Planktonic Foraminifera. Hutchinson Ross Publishing Company, Stroudsburg, p. 265.

Kennett, J.P., Huddlestun, P., 1972. Late Pleistocene paleoclimatology, foraminiferal biostratigraphy, and tephrochronology, Western Gulf of Mexico. Quat. Res. 2, 38–69.

Kohl, B., Fillon, R.H., Roberts, H.H., 2004. Foraminiferal biostratigraphy and paleoenvironments of the Pleistocene lagniappe delta and related section, northeastern Gulf of Mexico. In: Anderson, B., Fillon, R.H. (Eds.), Late Quaternary Stratigraphic Evolution of the Northern Gulf of Mexico Margin, vol. 79. Society for Sedimentary Geology, pp. 190–216.

Langner, M., Mulitza, S., 2019. Technical Note: PaleoDataView – a software toolbox for the collection, homogenization, and visualization of marine proxy data. Clim. Past 15, 2067–2072. https://doi.org/10.5194/cp-15-2067-2019.

Le, J., Shackleton, N.J., 1992. Carbonate dissolution fluctuations in the western equatorial Pacific during the late Quaternary. Paleoceanography 7 (1), 21–42.

Leipnitz, I.I., Silva, J.L.L., Leipnitz, B., Aguiar, E.S., Leão, C.J., Giovanoni, L., Ferreira, F., 2005. Métodos para o trabalho com microfósseis e formas atuais. In: Timm, L.L., Cademartoti, C.V. (Eds.), Cadernos La Salle XI - Métodos de Estudo em Biologia, vol. 2, pp. 49–58, 1.

Lisiecki, L., Raymo, M.E., 2005. A Pliocene-Pleistocene stack of 57 globally distributed benthic $\delta^{18}O$ records. Paleoceanography 20, PA1003. https://doi.org/10.1029/2004PA001071.

Locarnini, R.A., Mishonov, A.V., Baranova, O.K., Boyer, T.P., Zweng, M.M., Garcia, H.E., Reagan, J.R., Seidov, D., Weathers, K., Paver, C.R., Smolyar, I., 2018. In: Mishonov Technical, A. (Ed.), World Ocean Atlas 2018, Volume 1: Temperature, NOAA Atlas NESDIS, vol. 81, p. 52.

Lourens, L.J., Hilgen, F.J., Shacketon, N.J., Laskar, J., Wilson, D., 2004. The Neogene period. In: Gradstein, F.M., Ogg, J.G., Smith, A.G. (Eds.), Geological Time Scale 2004. Cambridge University Press, pp. 409–440.

Lux, M., Mercier, H., Arhan, M., 2001. Interhemispheric exchanges of mass and heat in the Atlantic ocean in january–March 1993. Deep-Sea Res. 48, 605–638.

Marchito, T.M., Curry, W.B., Lynch-Stieglitz, J., Bryan, S.P., Cobb, K.M., Lund, D.C., 2014. Improved oxygen isotope temperature calibrations for cosmopolitan benthic foraminifera. Geochem. Cosmochim. Acta 130, 1–11.

Martin, R.E., Johnson, G.W., Neff, E.D., Krantz, D.E., 1990. Quaternary planktonic foraminiferal assemblage zones of the northeast Gulf of México, Colombia basin (Caribbean Sea), and tropical Atlantic Ocean: graphic correlation of microfossil and oxygen isotope datums. Paleoceanography 5 (4), 531–555.

Martin, R.E., Neff, E.D., Johnson, G.W., Krantz, D.E., 1993. Biostratigraphic expression of Pleistocene sequence boundaries, Gulf of Mexico. Palaios 8, 155–171.

Martinez, J.I., Mora, G., Barrows, T.T., 2007. Paleoceanographic conditions in the Western Caribbean Sea for the last 560 ka as inferred from planktonic foraminifera. Mar. Micropaleontol. 64, 177–188.

Mix, A.C., Le, J., Shackleton, N.J., 1995. Benthic foraminiferal stable isotopes stratigraphy of Site 846: 0-1.8 Ma. In: Pisias, N.G., Mayer, L.A., Janecek, T.R., Palmer-Julson, A., van Andel, T.H. (Eds.), Proceedings of the Ocean Drilling Program, vol. 138. Scientific Results.

Nace, T.E., Baker, P.A., Dwyer, G.S., Silva, C.G., Rigsby, C.A., Burns, S.J., Giosan, L., Otto-Bliesner, B., Liu, Z., Zhu, J., 2014. The role of North Brazil Current transport in the paleoclimate of the Brazilian Nordeste margin and paleoceanography of the western tropical Atlantic during the late Quaternary. Palaeogeogr. Palaeoclimatol. Palaeoecol. 415, 3–13, 0.

Nishi, H., Norris, R.D., Okada, H., 2000. Paleoceanographic changes in the dynamics of subtropical surface conditions at Hole 997A. In: Paull, C.K., Matsumoto, R., Wallace, P.J., Dillon, W.P. (Eds.), Proceedings of the Ocean Drilling Program, vol. 164. Scientific Results.

Ogg, J.G., 2020. Chapter 5 - geomagnetic polarity time scale. In: Gradstein, F.M., Ogg, J. G., Schmitz, M.D., Ogg, G.M. (Eds.), Geologic Time Scale 2020. Elsevier, ISBN 9780128243602, pp. 159–192. https://doi.org/10.1016/B978-0-12-824360-2.00005-X.

Patterson, R.T., Fishbein, E., 1989. Re-Examination of the statistical methods used to determine the number of point counts needed for micropaleontological quantitative research. J. Paleontol. 63, 245–248.

Peeters, F.J., Acheson, R., Brummer, G.-J.A., Rujiter, W.P.M., Schneider, R.R., Ganssen, G.M., Ufker, E., Kroon, D., 2004. Vigorous exchange between the Indian and Atlantic oceans at the end of the past five glacial periods. Nature 430, 661–665.

Peterson, R.G., Stramma, L., 1991. Upper-level circulation in the south Atlantic ocean. Prog. Oceanogr. 26, 1–73.

Portilho-Ramos, R.C., Barbosa, C.F., Rios-Netto, A.M., 2014. Planktonic foraminiferal variations in the southwestern Atlantic since the last glacial-interglacial cycle. Palaios 29, 38–44. https://doi.org/10.2110/palo.2012.104.

Prell, W.L., Damuth, J.E., 1978. The climate-related diachronous disappearance of Pulleniatina obliquiloculata in Late Quaternary sediments of the Atlantic and Caribbean. Mar. Micropaleontol. 3, 267–277.

Railsback, L.B., Gibbard, P.L., Head, M.J., Voaristsoa, N.R.G., Toucanne, S., 2015. Na optimized scheme of lettered marine isotopic stages for the last 1.0 million years, and the climatostratigraphic nature of isotope stage and substages. Quat. Sci. Rev. 111, 94–106.

Reimer, P.J., Bard, E., Bayliss, A., Beck, J.W., Blackwell, P.G., Ramsey, C.B., Buck, C.E., Edwards, R.L., Friedrich, M., Grootes, P.M., Guilderson, T.P., Haflidason, H., Hajdas, I., Hatté, C., Heaton, T.J., Hoffmann, D.L., Hogg, A.G., Hughen, K.A., Kaiser, K.F., Kromer, B., Manning, S.W., Niu, M., Reimer, R.W., Richards, D.A., Scott, E.M., Southon, J.R., Staff, R.A., Turney, C.S.M., van der Plicht, J., 2013. INTCAL13 and MARINE13 radiocarbon age calibration curves 0–50,000 Years cal BP. Radiocarbon 55 (4), 1869–1887.

Richardson, P.L., Hufford, G.E., Limeburner, R., Brown, W.S., 1994. North Brazil Current retroflection eddies. J. Geophys. Res. 99, 5081–5093.

Schott, F., Stramma, L., Fischer, J., 1995. The warm water inflow into the western tropical Atlantic boundary regime, spring 1994. J. Geophys. Res. 100, 24745–24760.

Shackleton, N.J., Berger, A., Peltier, W.R., 1990. An alternative astronomical calibration of the lower Pleistocene timescale based on ODP Site 677. Philosophical Transactions of the Royal Society of Edinburgh, Earth Sciences 81, 251–261.

Srinivasan, M.S., Sinha, D.K., 1992. Late Neogene planktonic foraminiferal events of the southwest Pacific and Indian Ocean: a comparison. In: Tsuchi, R., Ingle Jr., J.C. (Eds.), Pacific Neogene Environment, Evolution and Events: Tokyo. University of Tokyo Press, pp. 203–220.

Stainforth, R.M., Lamb, J.L., Luterbaqcher, H., Beard, J.H., Jeffords, R.M., 1975. Cenozoic planktonic foraminiferal zonation and characteristics of index forms. In: Paleontological Contributions, vol. 62. University of Kansas Press, Lawrence, p. 425.

Stow, D.A.V., Aksu, A.E., 1978. Disturbances in soft sediments due to piston coring. Mar. Geol. 28, 135–144.

Stramma, L., Fischer, J., Reppin, J., 1995. The North Brazil undercurrent. Deep Sea Res. 42, 773–795.

Talley, L., Pickard, G., Emery, W., Swift, J., 2011. Descriptive Physical Oceanography: an Introduction. Elsevier Academic, Boston, p. 560.

Thunnell, R.C., 1984. Pleistocene planktonic foraminiferal biostratigraphy and paleoclimatology of the Gulf of México. In: Healy-Williams, N. (Ed.), Principles of Pleistocene Stratigraphy Applied to the Gulf of Mexico. Boston. International Human Resources Development Corporation, pp. 25–64.

Toledo, F.A.L., Quadros, J.P., Camilo Jr., E., Santarosa, A.C.A., Flores, J.A., Costa, K.B., 2016. Plankton biochronology for the last 772,000 years from the western South Atlantic ocean. Mar. Micropaleontol. 127, 50–62. https://doi.org/10.1016/j.marmicro.2016.07.002.

Vicalvi, M.A., 1997. Zoneamento bioestratigráfico e paleoclimático dos sedimentos do Quaternário superior do talude da Bacia de Campos, RJ, Brasil. Bol. Geociencias Petrobras 11 (1), 132–165.

Wade, B.S., Pearson, P.N., Berggren, W.A., Pälike, H., 2011. Review and revision of Cenozoic tropical planktonic foraminífera biostratigraphy and calibration to the geomagnetic polarity and astronomical time scale. Earth Sci. Rev. 104, 111–142.

Wilkens, R.H., Westerhold, T., Drury, A.J., Lyle, M., Gorgas, T., Tian, J., 2017. Revisiting the Ceara Rise, equatorial Atlantic ocean: isotope stratigraphy of ODP Leg 154 from 0 to 5 Ma. Clim. Past 13, 779–793. https://doi.org/10.5194/cp-13-779-2017.

Wilson, K.E., Maslin, M.A., Burns, S.J., 2011. Evidence for a prolonged retroflection of the North Brazil Current during glacial stages. Palaeogeogr. Palaeoclimatol. Palaeoecol. 301 (1–4), 86–96. https://doi.org/10.1016/j.palaeo.2011.01.003.

Zhang, D., Msadek, R., McPhaden, M.J., Delworth, T., 2011. Multidecadal variability of the North Brazil Current and its connection to the Atlantic meridional overturning circulation. J. Geophys. Res. 116, C04012. https://doi.org/10.1029/2010JC006812.

Zhang, Y., Chiessi, C.M., Mulitza, S., Sawakuchic, A.O., Häggi, C., Zabel, M., Portilho-Ramos, R.C., Schefuß, E., Crivellari, S., Wefer, G., 2017. Different precipitation patterns across tropical South America during Heinrich and Dansgaard-Oeschger stadials. Quat. Sci. Rev. 177, 1–9. https://doi.org/10.1016/j.quascirev.2017.10.012.

Zhang, Y., Chiessi, C.M., Mulitza, S., Zabel, M., Trindade, R.I.F., Hollanda, M.H.B.M., Dantas, E.L., Govina, A., Tiedemann, R., Wefer, G., 2015. Origin of increased terrigenous supply to the NE SouthAmerican continental margin during Heinrich stadial 1 and the younger Dryas. Earth Planet Sci. Lett. 432, 493–500. https://doi.org/10.1016/j.epsl. 2015. 09.054.

Zweng, M.M., Reagan, J.R., Seidov, D., Boyer, T.P., Locarnini, R.A., Garcia, H.E., Mishonov, A.V., Baranova, O.K., Weathers, K., Paver, C.R., Smolyar, I., 2018. In: Mishonov Technical, A. (Ed.), World Ocean Atlas 2018, Volume 2: Salinity, NOAA Atlas NESDIS, vol. 82, p. 50.